Robotica (2015) volume 33, pp. 1568–1588. © Cambridge University Press 2014
doi:10.1017/S0263574714000897

Design and simulated characteristics of a new biped mechanism

Tao Li†,‡* and Marco Ceccarelli‡

†*Institute of Advanced Manufacturing Technology, Hefei Institutes of Physical Science, Chinese Academy of Sciences, Changzhou (Jiangsu) 213164, China*
‡*LARM: Laboratory of Robotics and Mechatronics, University of Cassino and South Latium, Via Di Biasio 43, Cassino 03043 (FR), Italy*

(Accepted March 11, 2014. First published online: April 15, 2014)

SUMMARY
This paper presents a new biped mechanism with low-cost easy-operation features. The mechanism is designed with functions for straight walking, changing direction, overcoming obstacle, and climbing stairs with only 7 DOFs (degrees of freedom). Dynamics of the biped mechanism are analyzed by means of simulations in the MSC.ADAMS environment. Simulation results in terms of motion torque, joint force, contact force, parts displacement, velocity, and acceleration are reported and analyzed to show the feasibility and efficiency of the proposed solution. In addition, with the simulation results, dynamical motion of the biped mechanism is investigated and its operation performances are characterized as well.

KEYWORDS: Humanoid robots; Biped mechanisms; Dynamic simulation; Walking modes; Motion capability.

1. Introduction

Usually, humanoid robots are designed with conventional 12-DOF (degrees of freedom) biped mechanisms with a 3-DOF hip, a 1-DOF knee, and a 2-DOF ankle for each leg. Examples can be found in the humanoid robots P3 and ASIMO[1] that were developed by HONDA; HRP-2[2,3] that was developed by the Japanese National Institute of Advanced Industrial Science and Technology and Kawada Industries, Inc.; H7[4] that was constructed by the University of Tokyo; KHR and HUBO series[5,6] that were developed at the Korea Advanced Institute of Science and Technology; and BHR-2[7] that was built by the Intelligent Robotics Institute at Beijing Institute of Technology. There are other humanoid robots designed with a 14-DOF leg mechanism, like, for example, WABIAN-2[8] that has been designed by Waseda University. The legs of these humanoid robots show an anthropomorphic motion capability due to the use of high-performance motors, high-capability controllers, and multiple sensors. However, these robots are not available for a wide variety of applications because of their high cost. On the other hand, some researchers devote attention to the designs with reduced-DOF biped mechanisms, which have advantages of low cost and easy operation mainly because fewer motors are used. Examples are PASIBOT, which was built in University Carlos III of Madrid, as a 1-DOF biped leg mechanism;[9] and Meltran II, which was developed by Mechanical Engineering Laboratory in Japan, as a 6-DOF biped leg mechanism.[10]

At LARM, Laboratory of Robotics and Mechatronics in the University of Cassino and South Latium, a research line is devoted to the design of low-cost easy-operation leg mechanisms. In the past, two 1-DOF biped leg mechanisms have been proposed and built[11–13] with linkage architecture, which can produce human-like walking gait. The above-mentioned biped robots are similar to their costly counterparts in the sense that they can offer possibilities to develop and improve new biped walking algorithms, but with reduced costs. Nevertheless, fewer motors make them not as flexible as their counterparts, and reduced DOF leg mechanisms cannot adjust walking gait, which leads to

* Corresponding author. E-mail: roboylee@163.com

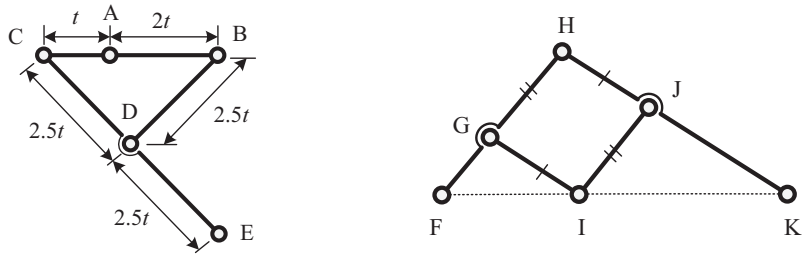

(a) (b)

Fig. 1. The two elementary mechanisms used for designing LARM leg series: (a) Chebyshev linkage; (b) pantograph linkage.

low walking capability, especially for changing direction, overcoming obstacles, and descending and ascending stairs.

Based on previous works on biped mechanisms at LARM, this paper presents a new biped mechanism, whose structure and design specifications are briefly introduced in Section 2. In particular, a dynamic analysis of three typical walking modes for straight walking, changing direction, and overcoming obstacle is discussed via simulations in ADAMS in Section 3. Simulation results are reported and analyzed with the aim to characterize motion performance of the biped mechanism. Finally, conclusions are outlined in Section 4.

2. Structure and Design Specifications

A Chebyshev linkage and a pantograph linkage are used as basic mechanisms in the leg. In Fig. 1(a), the Chebyshev linkage ABCDE is a four-bar mechanism with link length proportion as AB:AC:BD:CD:DE = 2:1:2:2.5:2.5, in which AB is a frame link, AC is an input crank, BD is a rocker, and CE is a coupler. The Chebyshev linkage is used as an input driving mechanism of a leg. It can generate an ovoid curve at the output joint E, which is very suitable for a walking gait of biped mechanisms, because the trajectory has an approximate straight-line segment that is related to the supporting phase, and it has a curved segment which is related to the swing phase of walking patterns. The pantograph linkage is used for amplifying the output trajectory of the Chebyshev linkage to a proper larger size. In Fig. 1(b), it is characterized by the parallelogram GIJH and collinear joints F, I, and K. Amplification ratio of the pantograph linkage depends on the length of bar FG and bar GH, and the configuration of input joint, output joint, and fixed joint.

The structure of the new biped mechanism is shown in Fig. 2. One motor is used for driving the Chebyshev linkage. Parallelograms are used with the aim to make the foot motion parallel to ground while walking. Each shank is composed of an upper part and a lower part in order to make its length adjustable. Sliders are assembled between the two parts and a linear screw motor is used for pulling/pushing the lower part of the shank. In order to make the biped mechanism possess the advantages of both legged and wheeled robots, a wheel is assembled on the upper part of each shank. Another motor is used to actuate the wheel. Another motor is used for changing direction. Thus, each leg has three motors and the biped mechanism has 7 DOFs in total. The left and right legs are designed with the same structure.

In Table I, main parameters of the leg mechanism are given with characteristic values for the proposed solution. In particular, the mass refers to the whole mechanical design; the dimensions in height and body size are assumed to reproduce a humanoid solution; the shank length refers to fully extended configuration; the foot length is the size given by the parallelogram together with ground contact constraints; the step sizes are obtained by considering the input motions for the actuators. These parameters are designed as referring to the dimensions of average human adults by taking into account that a biped robot can be used to provide service tasks for human beings. Those robot sizes will make the robot fit well with living environments of human beings. In addition, walking speed of this biped mechanism is considered as 0.36 m/s. This is the speed used in the simulations, while in real applications it could be increased or decreased easily by controlling the current in the motors.

https://doi.org/10.1017/S0263574714000897 Published online by Cambridge University Press

Table I. Specifications of new LARM 7-DOF biped mechanism in Fig. 2.

Parameter	Value
Total DOFs	7
Mass	18 kg
Height	0.96 m
Body length	0.22 m
Body width	0.36 m
Thigh length	0.27 m
Shank length	0.54 m (stretched)
Foot length	0.18 m
Step length	0.36 m
Step width	0.25 m
Walking speed	0.36 m/s

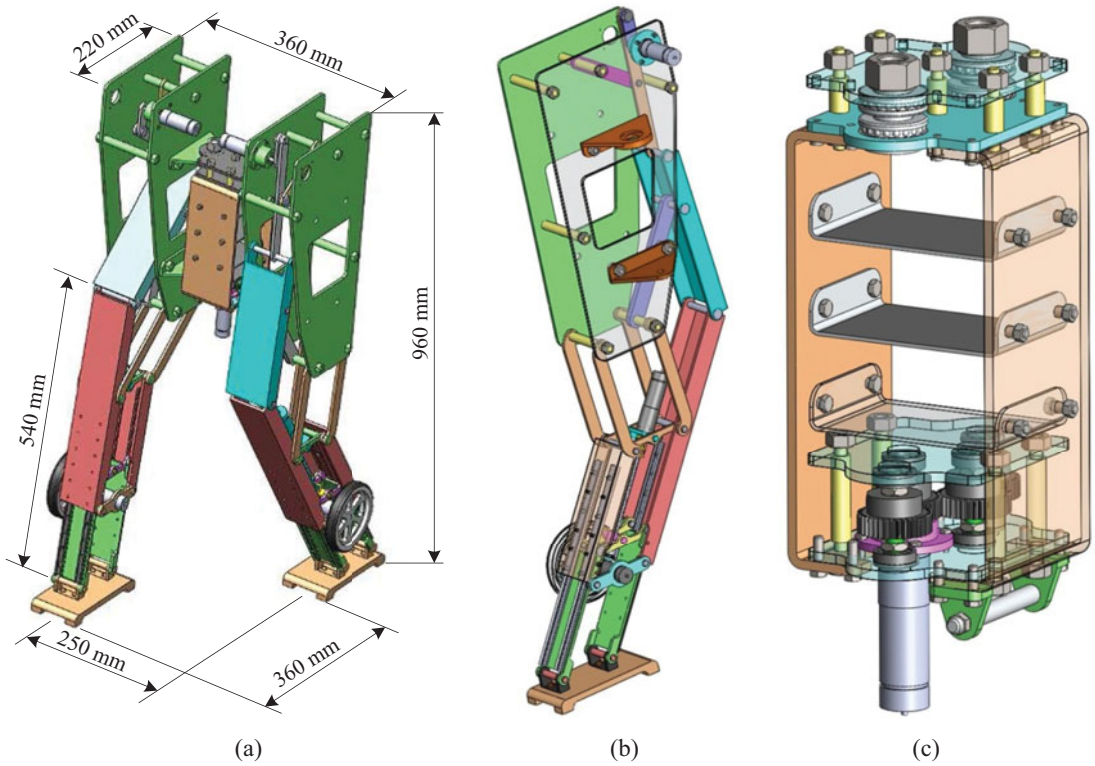

Fig. 2. Structure of the biped mechanism: (a) an overview of the biped mechanism with dimensions; (b) a detailed structure of one leg; (c) a detailed structure of the body.

The new proposed biped mechanism has four main novel characteristics:

- Comparing with conventional 12-DOF or 14-DOF biped robots, this new proposed biped mechanism has only seven motors. The reduced number of motors can give a low-cost design feature and fairly simple operation since the new biped mechanism can have the same basic functions for straight walking, changing direction, overcoming obstacle, and climbing stairs as in the solutions with the 12-DOF or 14-DOF legs.
- By using Chebyshev linkage, the new biped mechanism can generate a suitable walking gait automatically, and gait planning is not needed. By using a parallelogram in the shank, the foot moves always parallel to the ground during walking. Thus control of ankle joint in conventional biped robots is not needed for this new biped mechanism, by making it an easy-operation robot.
- Compared with existing 1-DOF biped robots, which can just make planar motion, this new biped mechanism can perform basic functions as conventional 12-DOF or 14-DOF biped robots can do.

https://doi.org/10.1017/S0263574714000897 Published online by Cambridge University Press

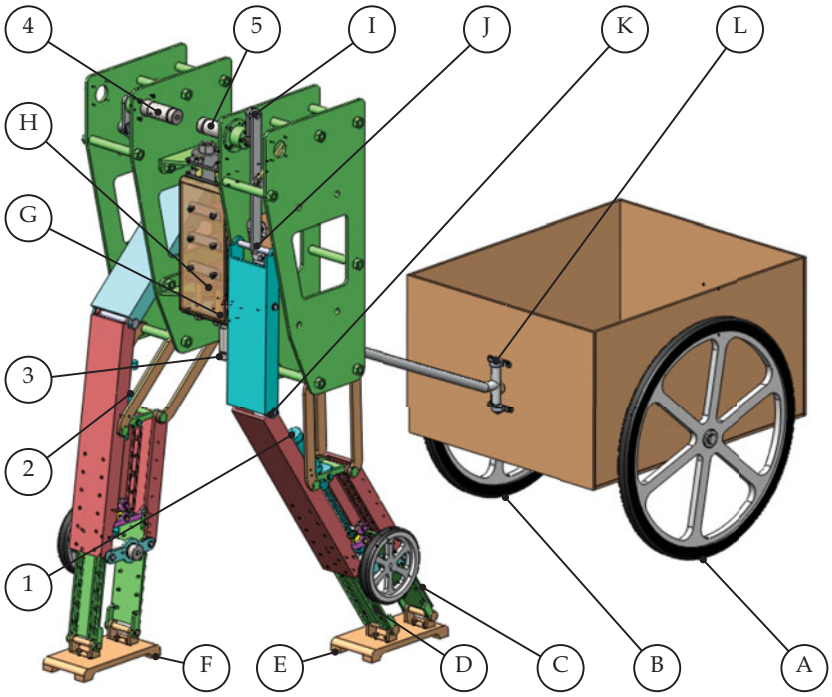

Fig. 3. A simulation model of the proposed biped mechanism in ADAMS: (1) motor for pulling/pushing left shank; (2) motor for pulling/pushing right shank; (3) motor for changing direction; (4) right leg driving motor; (5) left leg driving motor; constraint A: left wheel–ground contact (LWC); constraint B: right wheel–ground contact (RWC); constraint C: left shank rear slider (LSRS); constraint D: left shank front slider (LSFS); constraint E: left foot–ground contact (LFC); constraint F: right foot–ground contact (RFC); constraint G: motor–gear connecting joint (MGCJ); constraint H: leg–gear connecting joint (LGCJ); constraint I: left Chebyshev crank joint (LCCJ); constraint J: left Chebyshev output joint (LCOJ); constraint K: left knee joint (LKJ); constraint L: chariot connecting joint (CCJ).

These basic functions as changing directions, overcoming obstacle, and descending and ascending stairs are essential for biped robots to be used as service robots.

- With two additional wheels in the shank, the proposed biped mechanism can have two basic walking modes, namely the legged mode and wheeled mode. The robot can run a suitable walking mode according to environment situations. For example, when walking on flat ground without obstacles, it adopts wheeled mode, when meeting obstacles or stairs, it turns to legged mode. This possibility enables the robot to use wheels whenever convenient, and foot whenever needed. With this strategy the robot can possess the advantages of both legged robots and wheeled robots.

Thus, the novelty of the proposed design with the presented characteristics can be recognized in a mechanism-based design with fairly simple user-oriented operation. Furthermore, the robot is capable of walking on inclined planes with legged mode, because as pointed out in the second paragraph in this section, the foot is parallel to the ground while walking parallel to the robot body. In addition, it is easily capable of walking on inclined planes with wheeled mode.

3. Dynamic Simulations and Characterization of the Walking Modes

In order to simplify the simulation, simplification is made to the model in such a way: if there are no relative motions between a set of parts, this set of parts is joined as a single part. Nevertheless, shapes and mass distributions are still kept in the original model, so that the simplified model has the same outlook, mass distribution, and kinematic joints configuration as the original model and simulation is computed with the simplified model reflecting the original model.

The simplified model is imported into ADAMS first. Then materials are specified for each part. Finally kinematic joints are specified in terms of revolute joints, spherical joints, cylindrical joints,

https://doi.org/10.1017/S0263574714000897 Published online by Cambridge University Press

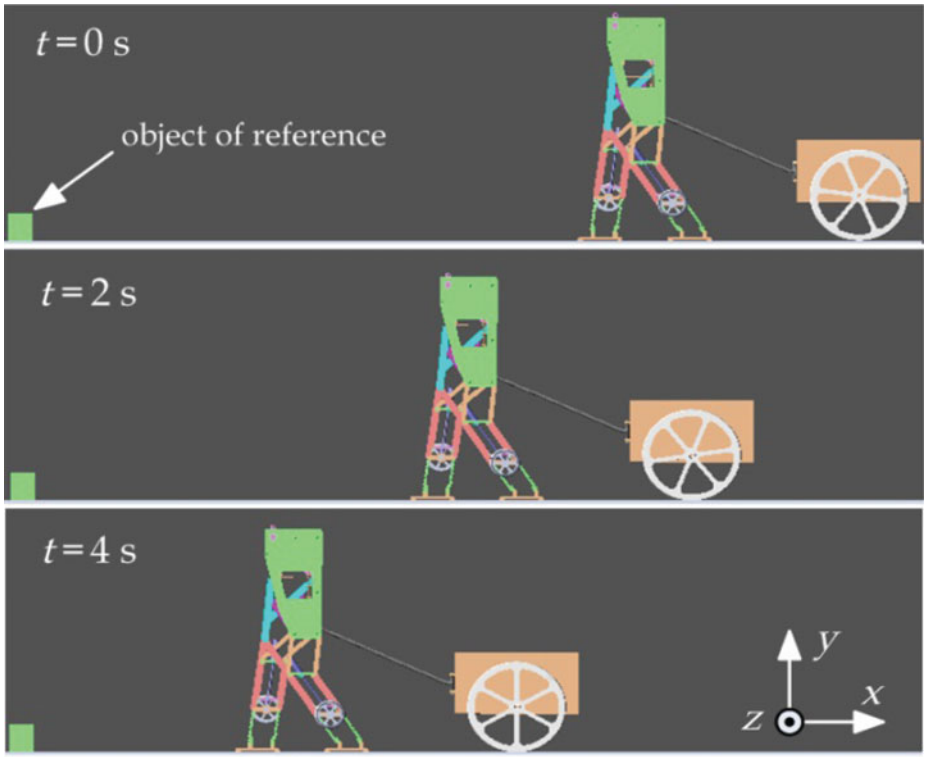

Fig. 4. Snapshots of simulation output of the straight walking mode (side view).

and translational joints. In particular, these joints are carefully modeled with the aim to eliminate any redundant constraint equations for feasible results. Contact types of feet or wheels with the ground are modeled as between solid bodies and solid; static coefficient and dynamic coefficient are assumed as 0.5 and 0.3, respectively. Stiction and sliding effect are used to model joint friction. The simulation model is computed as in Fig. 3. In particular, ground contact of the feet and wheels are modeled in the same way in order to keep symmetric feature of the biped mechanism.

The proposed robot design is aimed at generating the walking with fairly easy operation that is based on static equilibrium through the action of the chariot in order to avoid dynamic control as required for a bipedal motion. Thus, although zero moment point (ZMP) and dynamic stability are necessary for bipedal motion, in the presented solution they are avoided in favor of fairly simple user-oriented applications even with more significant payload capability. It is worth to note that in the simulation, only the motion capability of the biped mechanism is evaluated and the chariot is used with the aim to avoid complex control strategy. In particular, during the walking, the stability of the biped mechanism is guaranteed by the chariot, which provides two additional ground contact points in order to have always static stability conditions. This paper is not referring to biped control but focus on mechanism. The chariot is not only used with the aim to avoid complex control of the biped mechanism, but it has been considered useful for carrying high payload that in general is not possible by conventional biped robots.

3.1. Straight walking

Straight walking is one of the basic walking modes. When working in this mode, only the two motors of the legs work. The other five motors do not work or work in self-lock configuration. The shanks are fixed at maximal length. Two legs are fixed to the common body. Figure 4 shows snapshots of the simulation output. In the simulation, input angular velocity is set up to 180°/s. When the motor rotates 180°, the biped mechanism moves one step forward. Since the step length is 0.36 m, the walking velocity of the biped mechanism is equal to 0.36 m/s. With the help of the chariot, the biped robot can perform fast walk with static conditions for walk. In addition, it is not a ZMP-based humanoid robot, and a faster velocity than BHR or RH-1 is possible.

https://doi.org/10.1017/S0263574714000897 Published online by Cambridge University Press

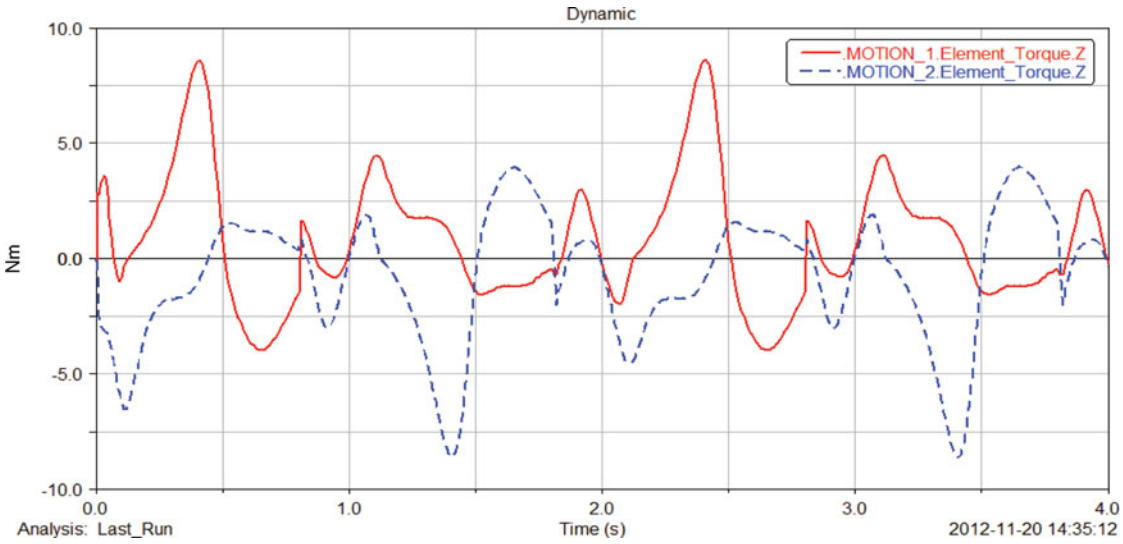

Fig. 5. Torque of the left leg motor (motor 4) and right leg motor (motor 5) as computed during the simulation in Fig. 4.

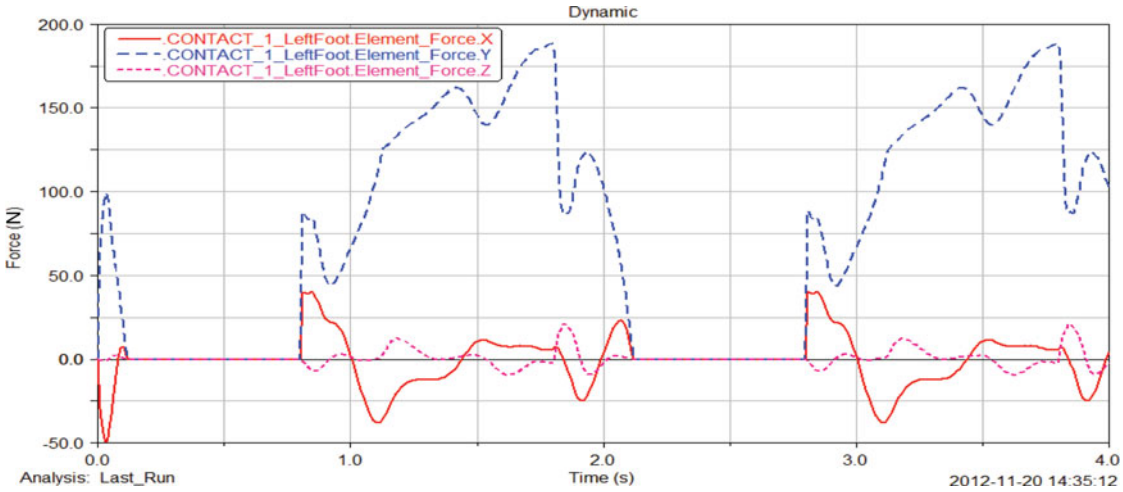

Fig. 6. *x*, *y*, and *z* components of the LFC force as computed during the simulation in Fig. 4.

Figure 5 shows the computed driving torque of motor 5 and motor 4 in Fig. 3, for which each leg walks two steps in 4 s. Plots show periodic operation and the time period of one walking cycle (two steps) is 2 s. Moreover, plots also show symmetric feature between the two legs. The torque is computed about *z*-axis, which is parallel to the axis of the motor shaft, and maximum value of the torque is computed as approximately 8.6 Nm. This value and smooth timeline of the driving torque give the possibility to choose market motors for a practical application with no critical requirements.

Figure 6 shows computed left foot–ground contact (LFC) force. Plots show that the force along *y*-axis, which is the vertical direction, is with the largest values as about 189 N. Since the mass of the biped mechanism is 18 kg, the values can be considered reasonable. Similarly, plots of the contact forces show periodic and symmetric features during walking. There are some periods during which the contact forces are zero, which represent the swing phases of the biped walking. In Fig. 6, the zero-value periods indicate the swing phases of the left foot. In such time periods, the right foot is in its supporting phases. The continuous dynamic response comes from the actuators that are assembled at the left and right crank joints as illustrated in Fig. 1 (number 4 and 5) rather than from the ground reaction force.

Since plots of the right foot–ground contact force and wheel–ground contact force show similar results, they are omitted. Similarly, in the following analysis in terms of joint force, displacement,

https://doi.org/10.1017/S0263574714000897 Published online by Cambridge University Press

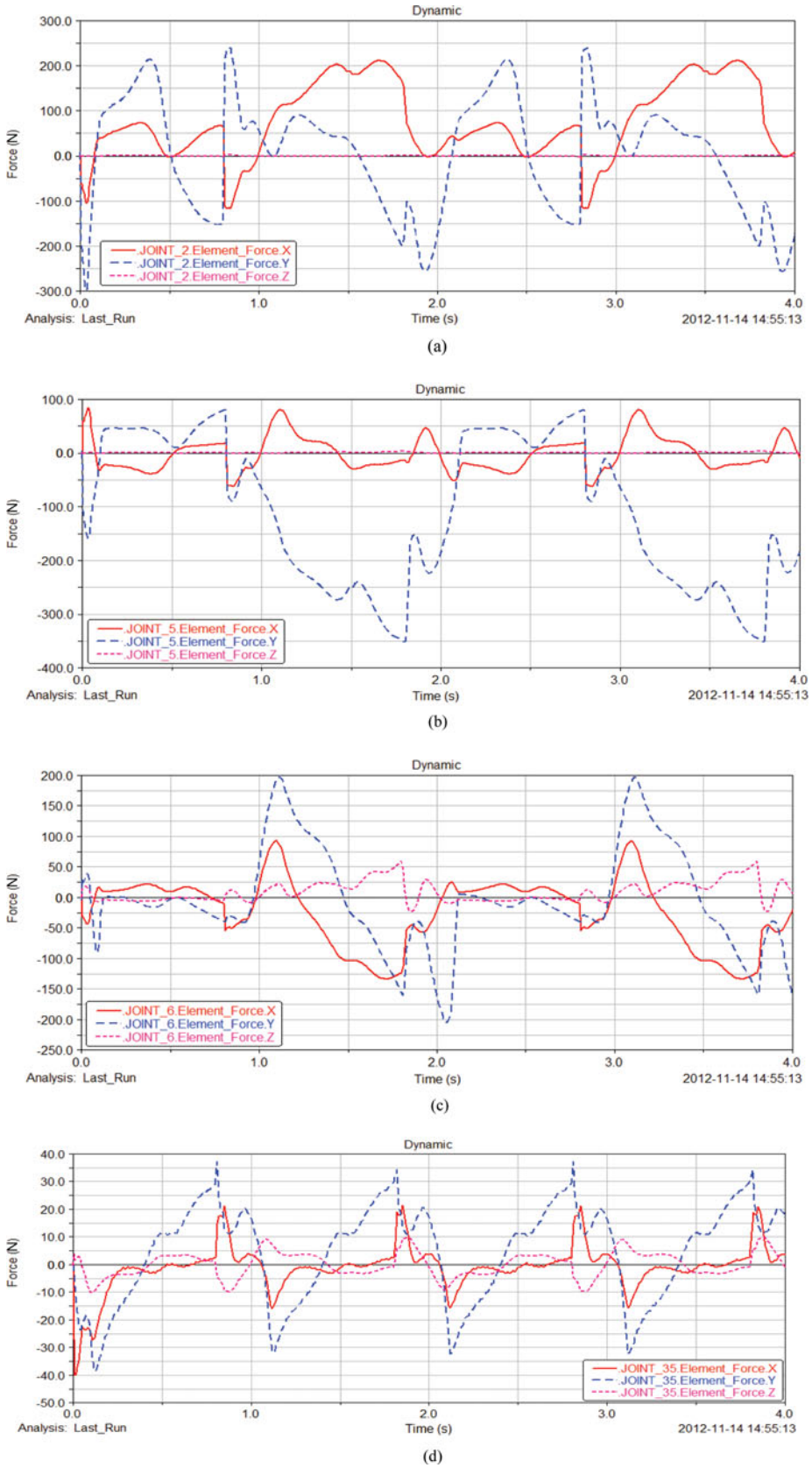

Fig. 7. *x*, *y*, and *z* components of joint force of: (a) LCCJ, (b) LCOJ, (c) LKJ, and (d) CCJ, as computed during the simulation in Fig. 4.

https://doi.org/10.1017/S0263574714000897 Published online by Cambridge University Press

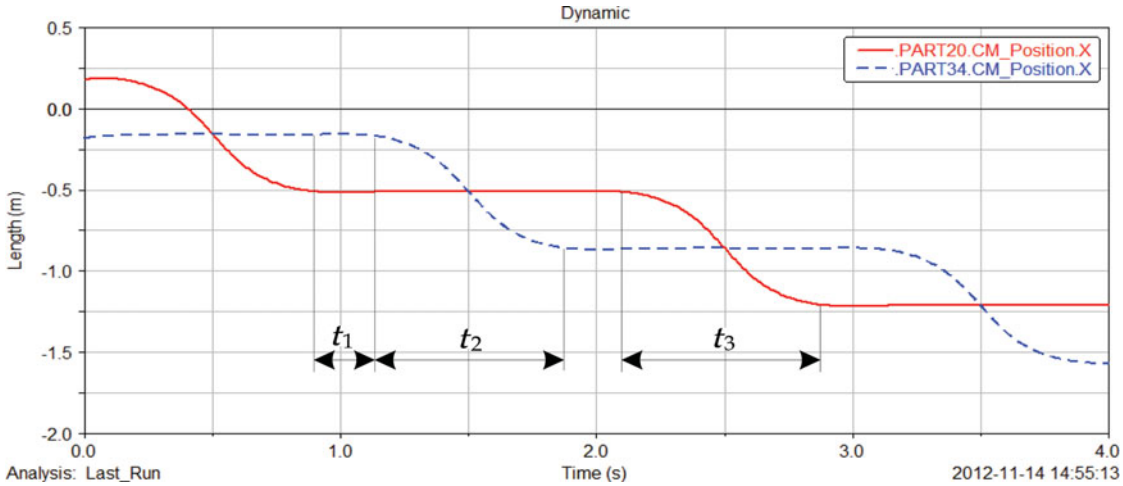

Fig. 8. CM distance of left and right feet from start position along walking direction during the simulation in Fig. 4.

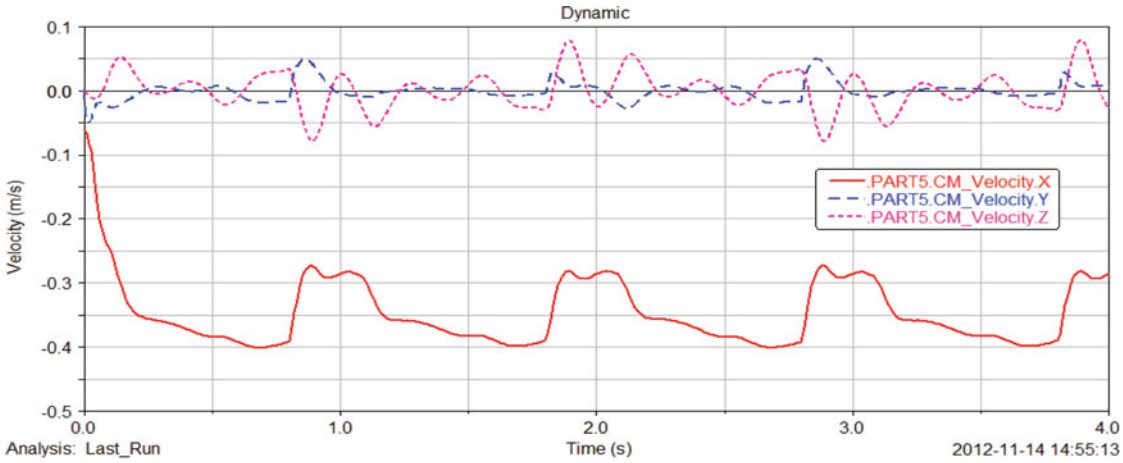

(a)

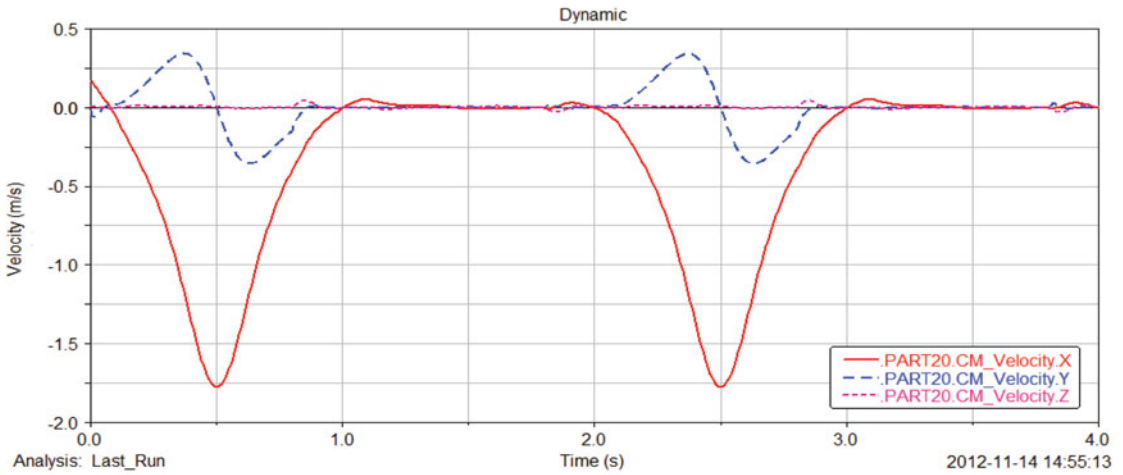

(b)

Fig. 9. Computed x, y, and z components of velocity of: (a) the body CM and (b) the left foot during the simulation in Fig. 4.

https://doi.org/10.1017/S0263574714000897 Published online by Cambridge University Press

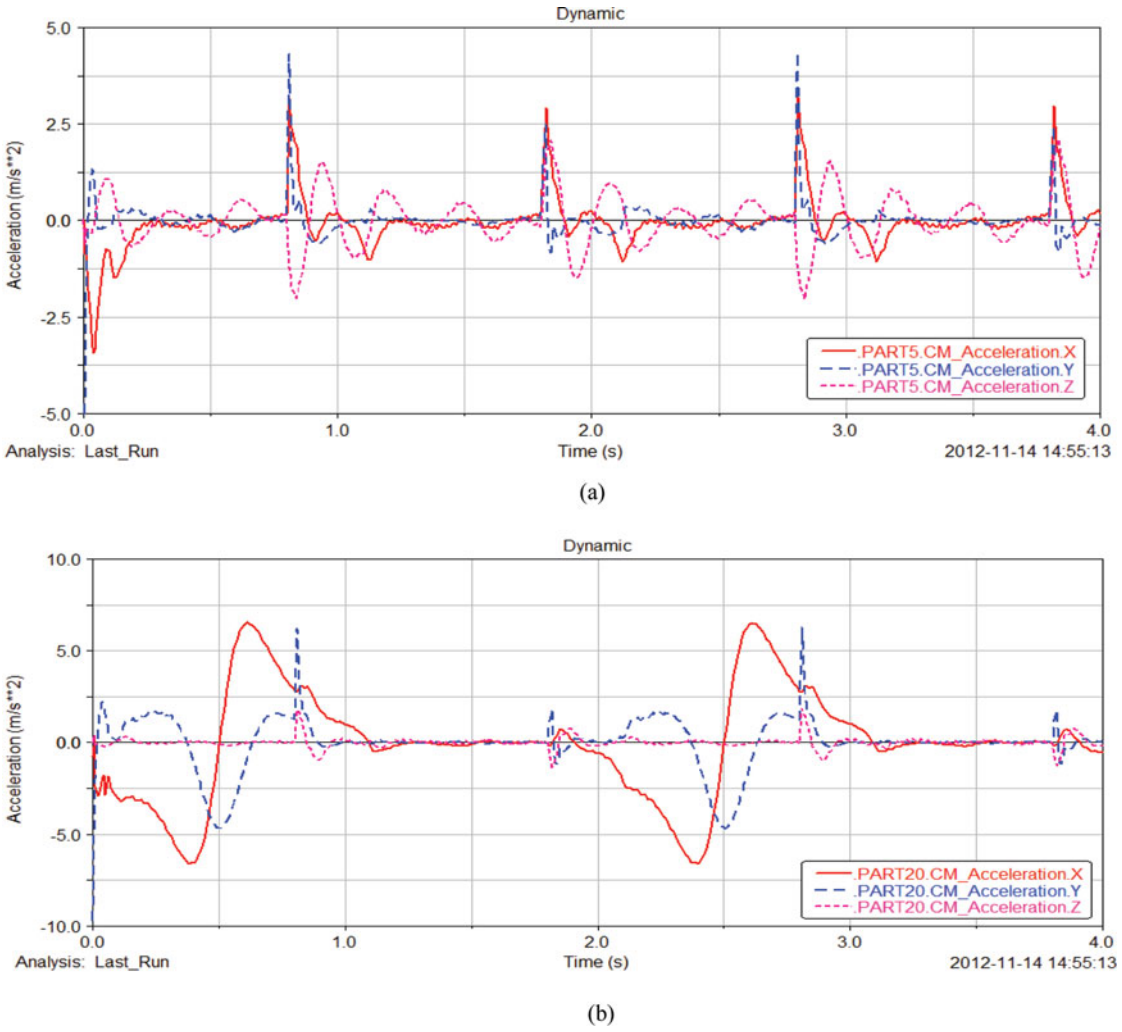

Fig. 10. Computed x, y, and z components of acceleration of: (a) the body CM and (b) the left foot during the simulation in Fig. 4.

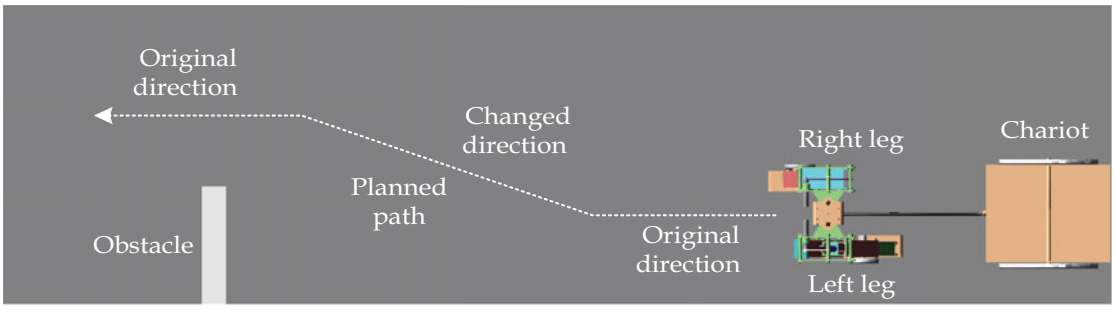

Fig. 11. A simulation scheme for changing direction with the aim to avoid an obstacle (top view).

velocity, and acceleration, only the results of one leg are shown and discussed since the two legs perform symmetric motions.

Figures 7(a)–7(d) show the x, y, and z components of reaction forces at the left Chebyshev crank joint (LCCJ), the left Chebyshev output joint (LCOJ), the left knee joint (LKJ), and the chariot connecting joint (CCJ), respectively. They are the key joints which work in relatively more critical situations than other joints. Maximum values of these joint forces in the plots are within feasible

https://doi.org/10.1017/S0263574714000897 Published online by Cambridge University Press

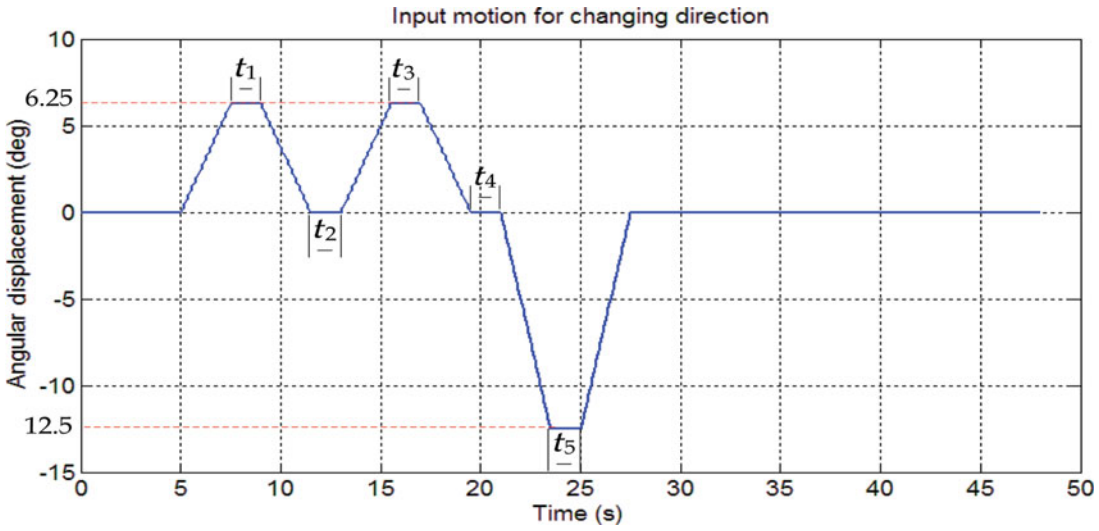

Fig. 12. Planned input motion of motor 3 for changing direction in the simulation of Fig. 15.

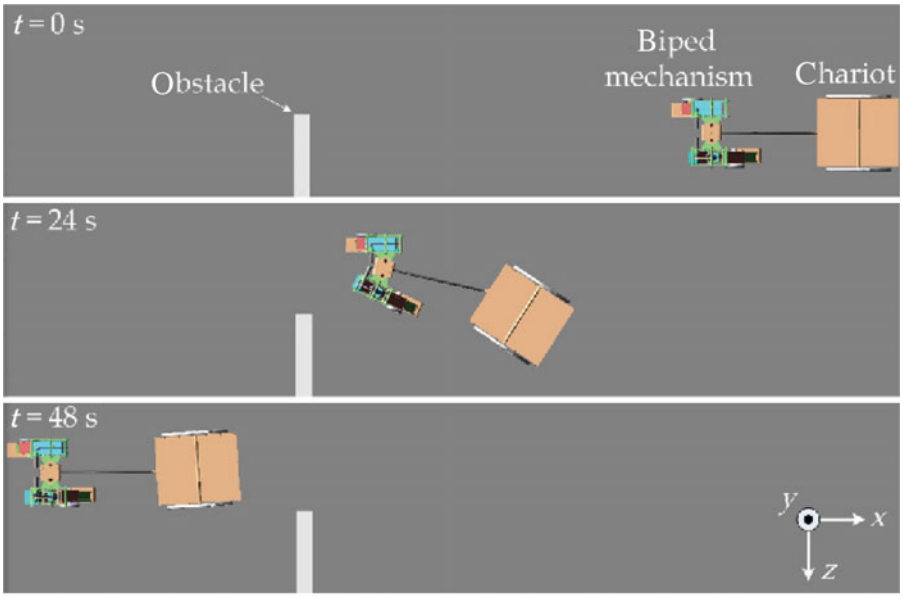

Fig. 13. Snapshots of simulation for changing direction in the simulation of Fig. 11.

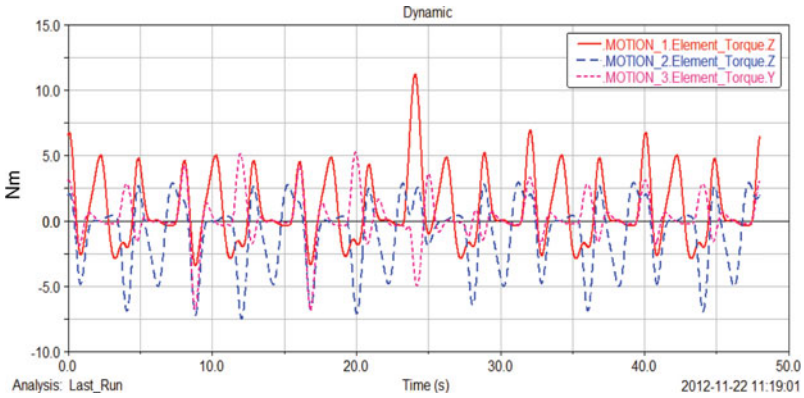

Fig. 14. Computed torques of motors 3, 4, and 5.

https://doi.org/10.1017/S0263574714000897 Published online by Cambridge University Press

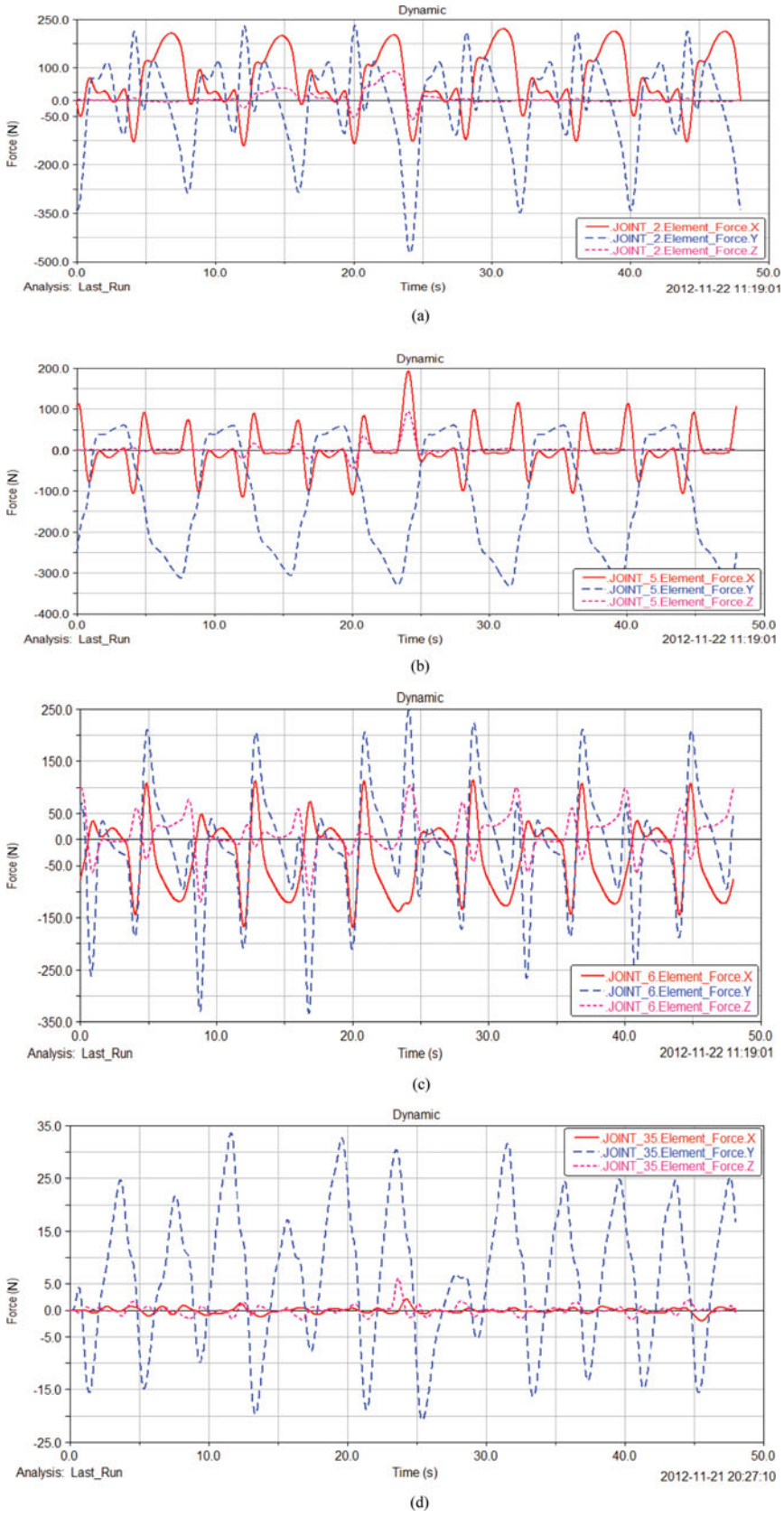

Fig. 15. *x*, *y*, and *z* components of joint force of: (a) LCCJ, (b) LCOJ, (c) LKJ, and (d) CCJ, as computed during the simulation in Fig. 13.

https://doi.org/10.1017/S0263574714000897 Published online by Cambridge University Press

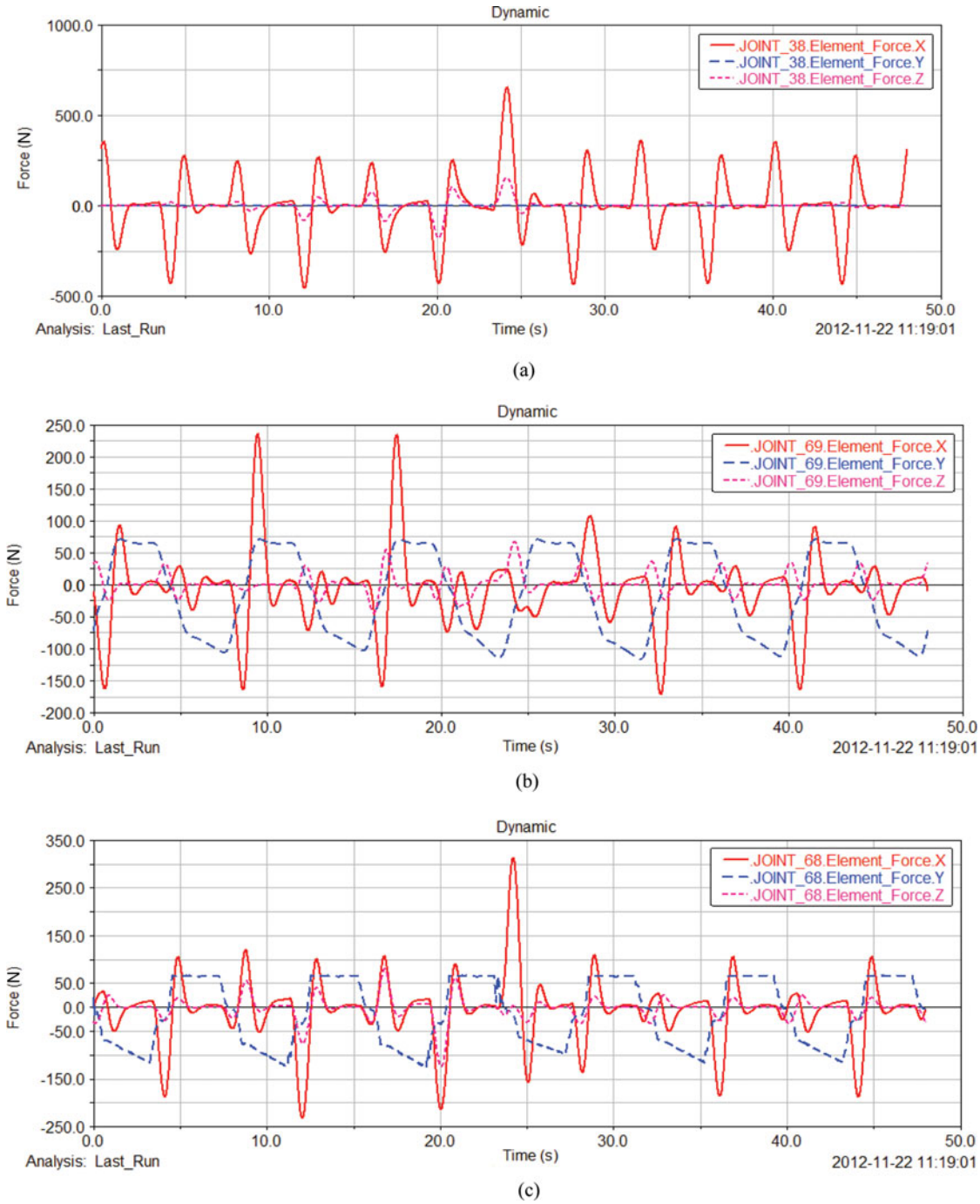

Fig. 16. *x*, *y*, and *z* components of the computed joint forces of: (a) the MGCJ, (b) the left LGCJ, and (c) the right LGCJ, as computed during the simulation in Fig. 13.

regions for the parts that are designed with proper dimensions and materials to resist the corresponding stress.

Simulation results show that the displacement of the leg body along the walking direction is nearly a straight line, with an approximately uniform motion. In addition, the leg body has minor displacement in vertical direction. These two aspects indicate that when the biped mechanism will be used as legs for a humanoid robot, the upper body of the robot will have a very smooth motion and have minor impact on the ground during walking.

https://doi.org/10.1017/S0263574714000897 Published online by Cambridge University Press

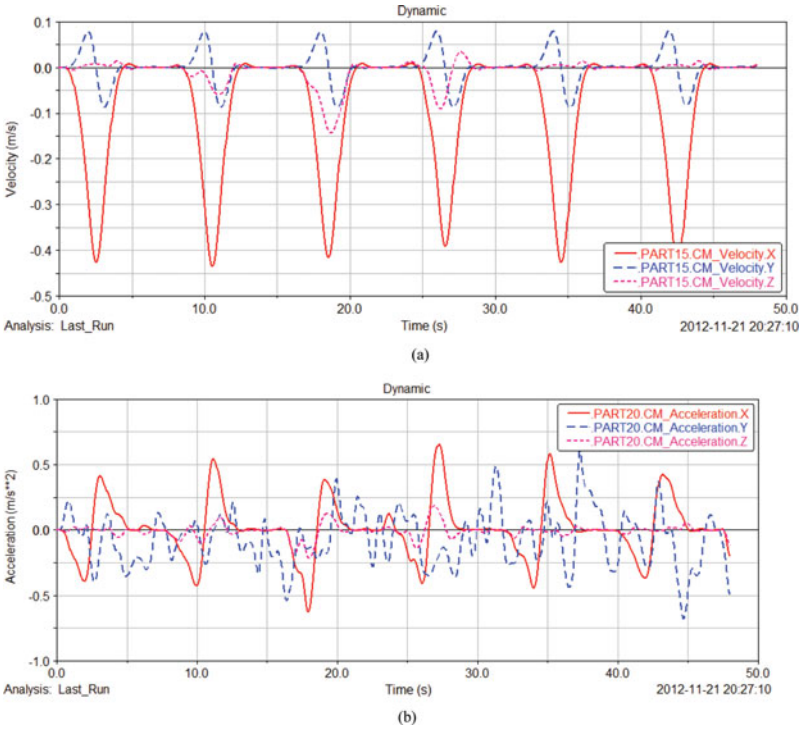

Fig. 17. Computed x, y, and z components of: (a) velocity of the left foot and (b) acceleration of the left foot, during the simulation in Fig. 13.

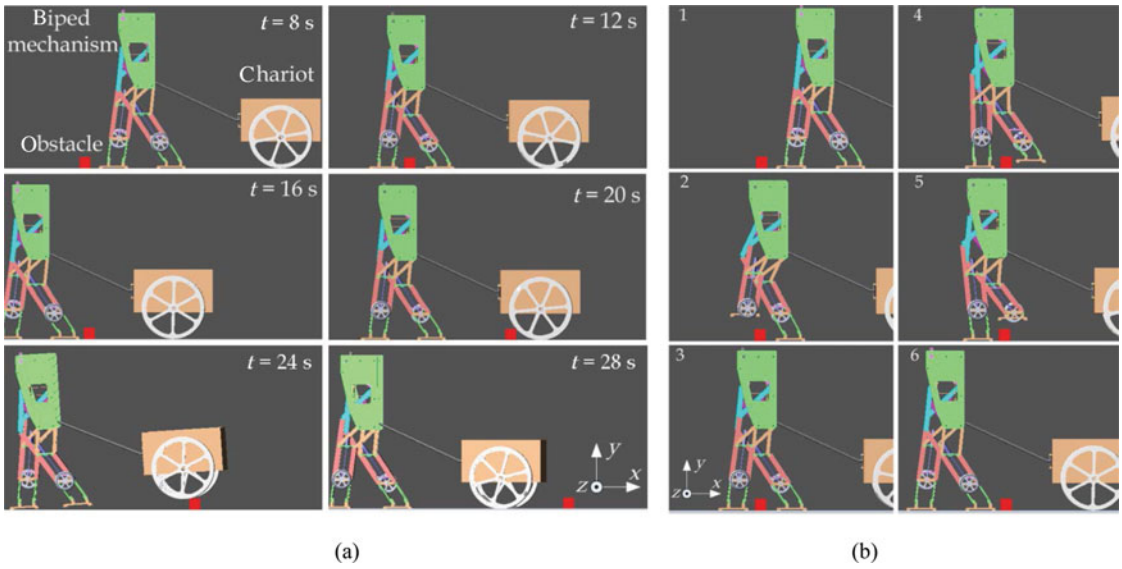

Fig. 18. Snapshots of simulation for overcoming an obstacle: (a) operation by the biped mechanism and chariot; (b) details for two legs (side view).

Figure 8 shows the CM (center of mass) distance of left and right feet from the start position along walking direction during the simulation in Fig. 4. Plots of the displacements of feet are step-shaped lines, with horizontal segments representing supporting phases and inclined parts representing swing phases. The time intervals t_1, t_2, and t_3 indicate double supporting phases, swing phase of the right leg and swing phase of the left leg, respectively. With a speed of about 0.36 m/s, the duration of supporting phase is about 1.2 s, whereas swing phase is about 0.8 s. Thus, supporting phase is longer than swing phase although it is in sequential order. Similar functioning can be found in human locomotion.

https://doi.org/10.1017/S0263574714000897 Published online by Cambridge University Press

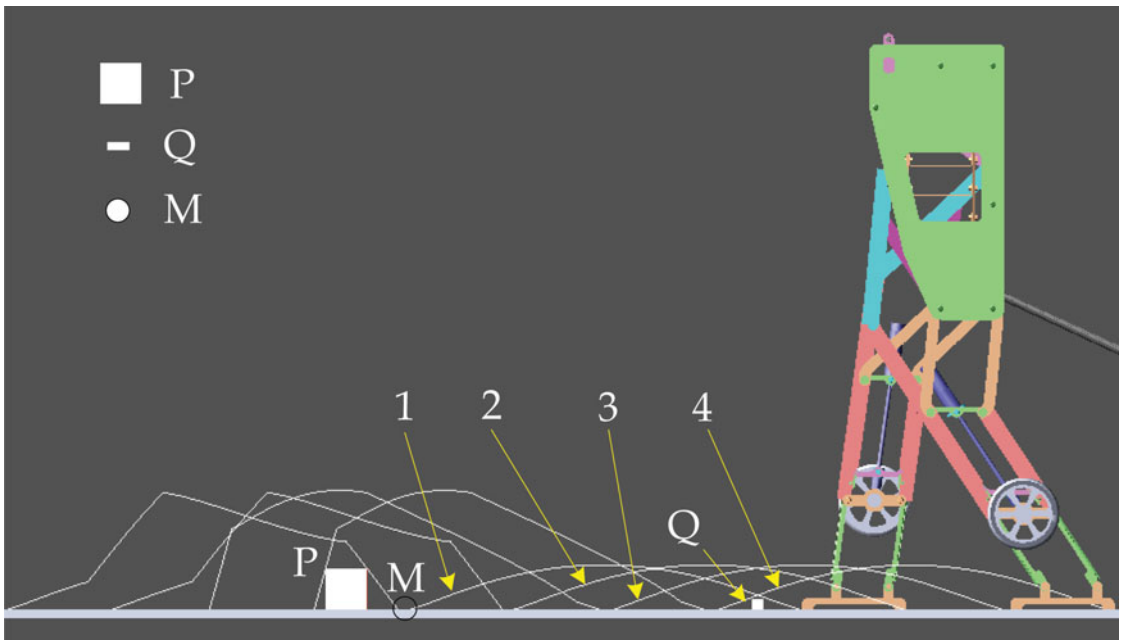

Fig. 19. A scheme for illustrating the obstacle overcoming capability of the biped mechanism with length-adjustable legs.

Figures 9(a), 9(b), 10(a), and 10(b) illustrate computed velocity and acceleration along x-axis (walking direction), y-axis (vertical direction), and z-axis (lateral direction) of the leg body and left foot during the simulation in Fig. 4, respectively. In particular, in Fig. 9, velocity of the leg body along the y and z axes is computed as very small, indicating that the body has minor motion in these two directions. Furthermore, the leg body has minimal velocity and acceleration, whereas foot has maximal velocity and acceleration, as expected for human-like operation. The computed values and plot shapes indicate that the biped mechanism has a fairly good motion performance with walking characteristics that are similar to those in human locomotion.

3.2. Changing direction

The second simulation refers to an operation for changing direction. There are two main reasons for a robot to change direction, namely, during a specified task, the path between a robot's initial location and its destination probably is not straight, and additionally, sometimes there are obstacles, which are not possible to overcome, although in front of the robot. Thus, changing direction can be considered as another basic walking mode. When working in this mode, motors work for driving two legs and for changing direction. The other four motors do not work or work in self-lock configuration. The shanks are fixed at maximal length. Each leg is assembled to the body through one revolute joint.

Operation principle for the mechanism to change direction is described in the first author's Ph.D. thesis.[14] In the reported simulation, the biped mechanism needs to change direction with the aim to avoid an obstacle lying in front of it. After avoiding the obstacle successfully, the biped mechanism turns back to its original direction. Namely, the biped mechanism needs to turn right first and then it turns left, as illustrated in the scheme of Fig. 11.

Figure 12 shows the used input motion of the motor for changing direction. The left leg moves one step forward, and then the right leg moves one step forward and turns right for 6.25° simultaneously. Then the left leg moves one step forward and turns right for 6.25° simultaneously. The two legs repeat the second and third steps and after then, the right leg moves one step forward and meanwhile turns to left for 12.5°. Finally, the left leg moves one step forward and turns to left for 12.5° in order to turn back to its original direction. It is worth to note that the operation of changing direction takes place during swing phases of the legs. During double supporting phase, the motor for changing direction has no rotation. In Fig. 12, t_1 to t_4 indicate durations of double supporting phases, during which the motor does not rotate. Figure 13 shows the snapshots of the simulated process with an angular

https://doi.org/10.1017/S0263574714000897 Published online by Cambridge University Press

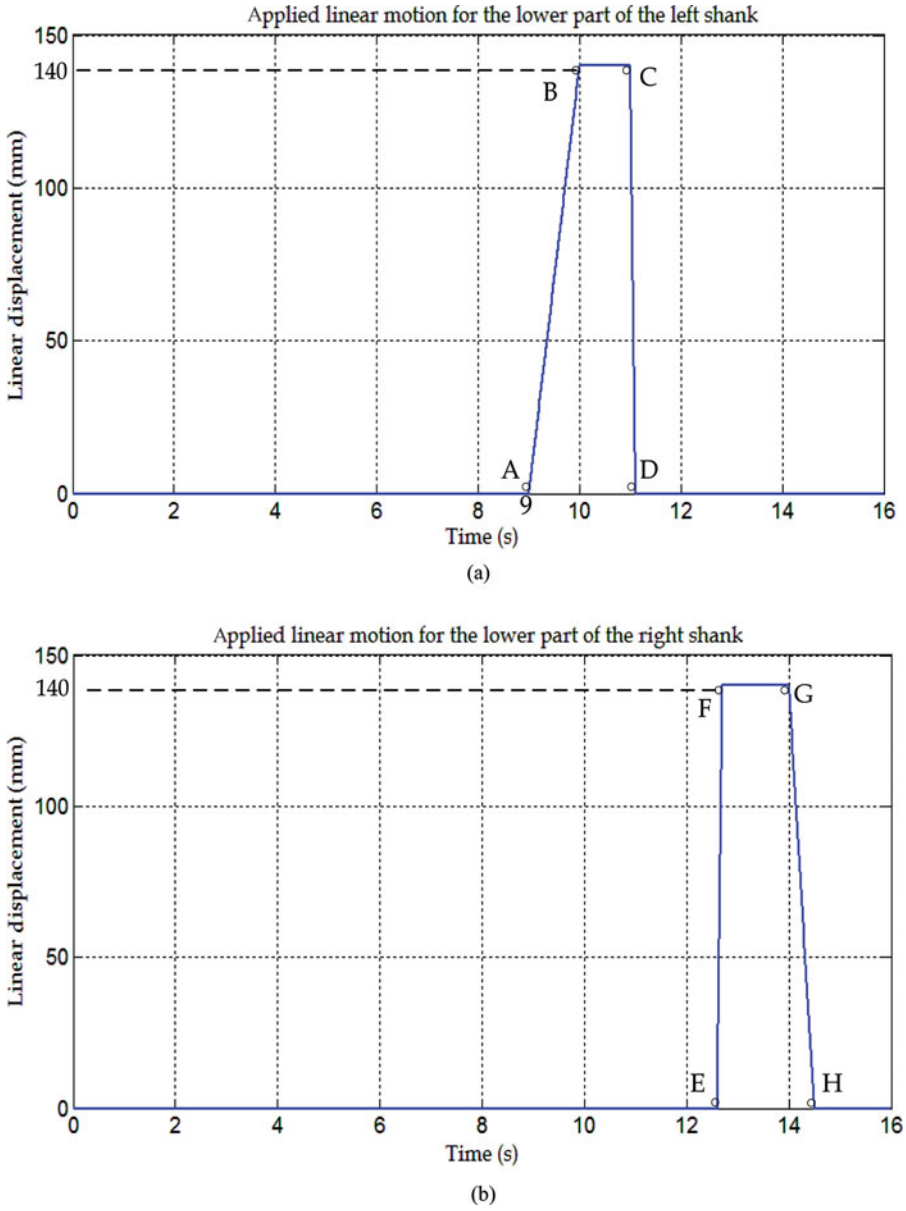

Fig. 20. Planned motion for the lower parts of the shanks in the simulation in Fig. 18: (a) motion for left leg; (b) motion for right leg.

velocity of the motor motion up to 45°/s. Simulation time is 48 s, during which each foot moves six steps.

Figure 14 shows the computed driving torque of motors 3, 4, and 5. The last two torques are computed about *z*-axis, and the first one is computed about *y*-axis. Maximum values of the driving torques are computed as equal to approximately 7 Nm, 7.5 Nm, and 11 Nm, respectively. The computed values and plot shapes can be considered feasible solution for commercial motors of proper power capability.

Simulation result of LFC force is larger than the computed one in the straight walking. This is because while changing direction, larger friction force is used for preventing foot sliding. Values of the wheel–ground contact force are similar to those that are computed in the first simulation.

Figures 15(a)–15(d) show the *x*, *y*, and *z* components of reaction forces at LCCJ, LCOJ, LKJ, and CCJ, respectively. Like in the previous simulation, the computed results give acting forces that can be considered with a proper level for the parts with the chosen materials.

https://doi.org/10.1017/S0263574714000897 Published online by Cambridge University Press

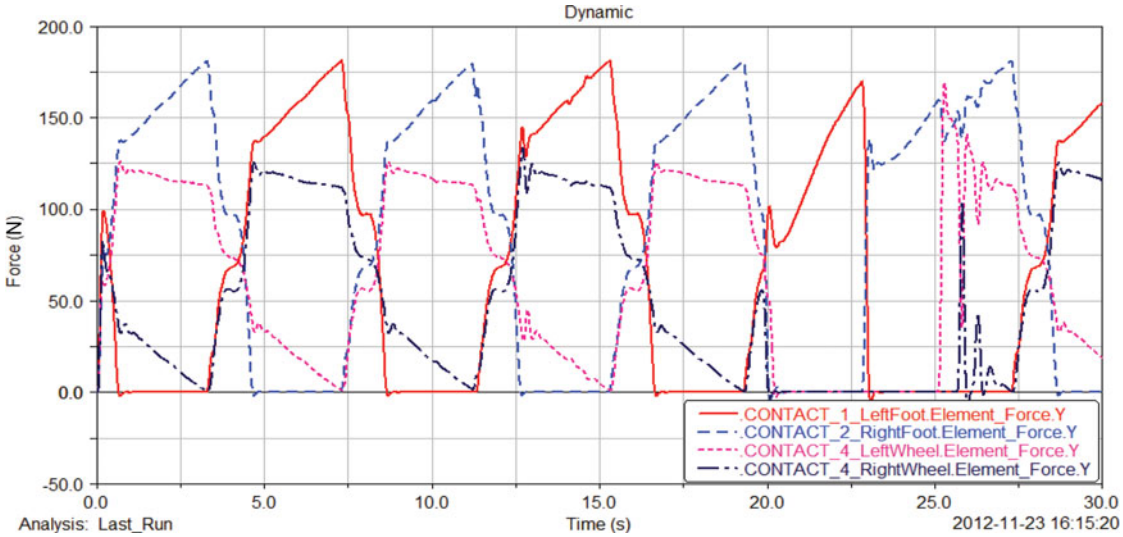

Fig. 21. Contact forces of the LFC, RFC, LWC, and RWC as computed during the simulation in Fig. 18.

Figure 16 shows computed joint forces at the four gears that are assembled in the mechanism for changing direction. In particular, Fig. 16(a) shows the force of the motor–gear connecting joint (MGCJ). Figs. 16(b) and 16(c) show the forces of the left and right leg–gear connecting joints (LGCJ), respectively. The computed maximum value is about 600 N. This force value can be considered feasible for the chosen commercial gears made in copper, as related to their transmission efficient capability.

Figures 17(a) and 17(b) show computed velocity and acceleration along walking direction, vertical direction, and lateral direction of the left foot during the simulation in Fig. 13. In particular, in Fig. 17(a), velocity of the left foot along y and z axes is very small, with a very smooth motion of the leg body even in the changing direction mode. In this case, the computed values and plot shapes indicate a fairly good performance in the operation with characteristics that are similar to that in human locomotion. Simulation results of velocity and acceleration of other parts are omitted since they do not show significant differences.

3.3. Overcoming obstacle

When a leg overcomes an obstacle, the two motors for actuating the shank wheels do not work, the motor for changing direction works at self-lock situation, and the other four motors for driving legs and shanks rotate. The shank length is adjustable because of the driving of the shank motors. Both legs are fixed to the leg body. Figure 18(a) shows snapshots of the simulation process from 8 s to 28 s. During the process, the biped mechanism overpasses the obstacle first, and then it pulls the chariot to overpass the obstacle successfully. Figure 18(b) shows details in overpassing the obstacle especially by the two legs.

Figure 19 illustrates the trajectories of the extreme points of feet as generated during the simulation. Numbers 1, 2, 3, and 4 represent the trajectories of the front and rear extreme points of the right and left feet, respectively. Box P is the obstacle that is overpassed during the simulation, while box Q is a reference obstacle which can be overpassed by stretched legs. Obviously, with adjustable shank, the biped mechanism can overcome an obstacle which has much larger dimensions (P) than the one that stretched legs can overcome (Q). Point M is a suitable touchdown point of the right leg. During the simulation, the biped mechanism is supposed to have the ability to reach such a point and to measure the size of the obstacle with the help of additional sensing devices that can be installed on the robot body. The simulation is focused on dynamic implementation and motion strategy by assuming that the biped mechanism has been properly equipped with sensors.

For the simulation, the input motions for the left and right shank motors are illustrated in Figs. 20(a) and 20(b), respectively. For the motion of the left shank in Fig. 20(a), time at points

https://doi.org/10.1017/S0263574714000897 Published online by Cambridge University Press

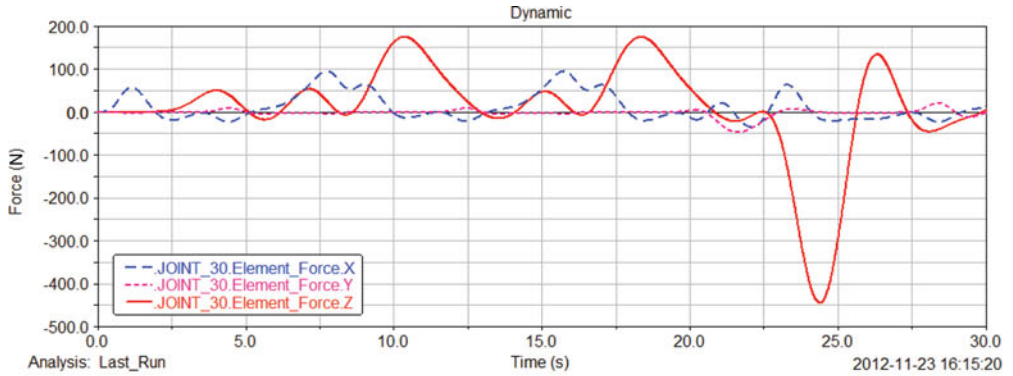

(a)

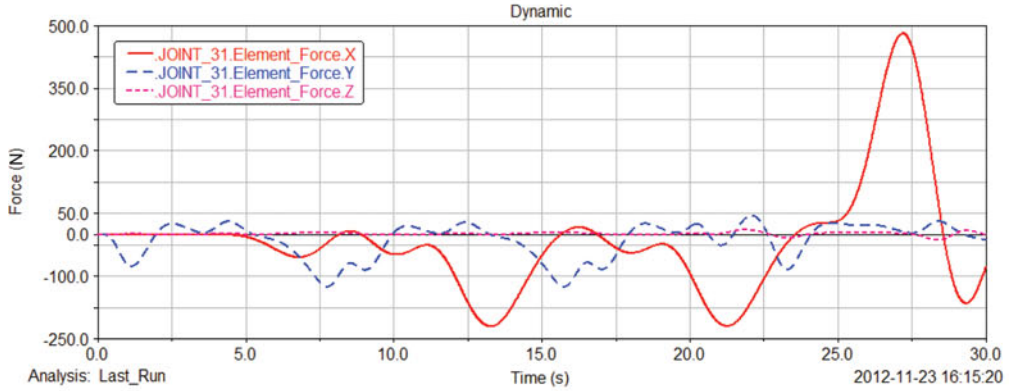

(b)

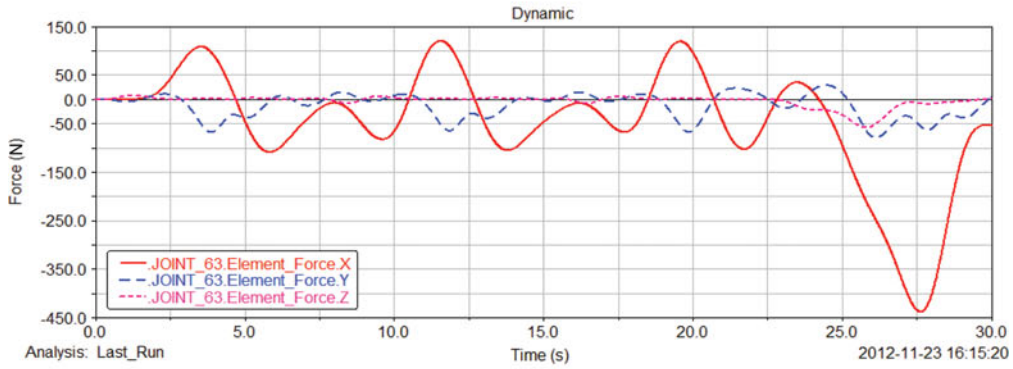

(c)

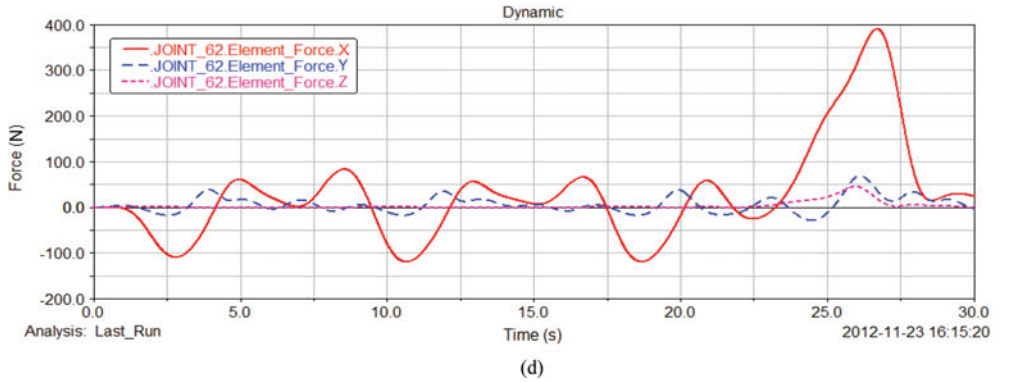

(d)

Fig. 22. *x*, *y*, and *z* components of joint force of sliders as computed during the simulation in Fig. 18: (a) joint force of the LSFS; (b) joint force of the LSRS; (c) joint force of the RSFS; (d) joint force of the RSRS.

https://doi.org/10.1017/S0263574714000897 Published online by Cambridge University Press

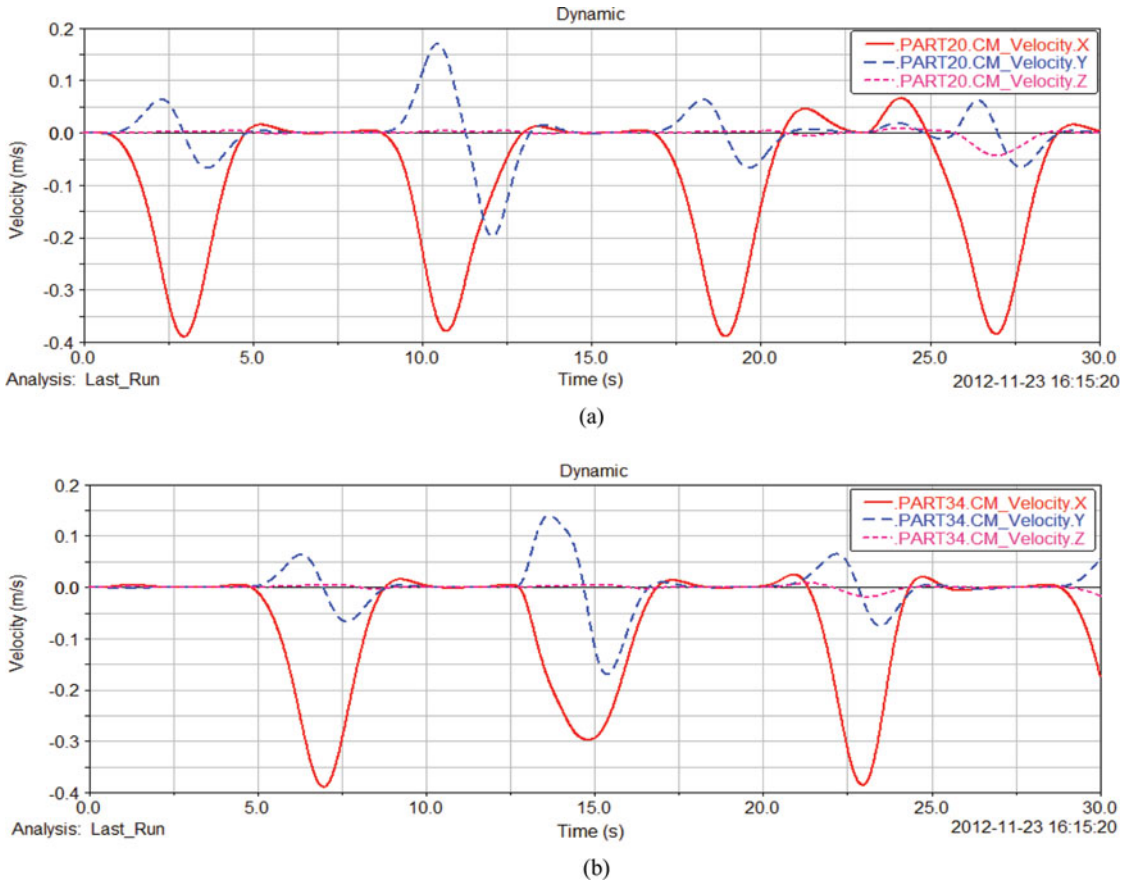

Fig. 23. *x*, *y*, and *z* components of CM velocity as computed during the simulation in Fig. 18: (a) the left foot CM velocity; (b) the right foot CM velocity.

A, B, C, and D is 9 s, 10 s, 11 s and 11.1 s, respectively. From A to B, the motor moves 0.14 m in 1 s with a velocity of 0.14 m/s. From C to D, it moves 0.14 m in 0.1 s with a velocity of 1.4 m/s. For the motion of the right shank in Fig. 20(b), time at points E, F, G, and H is 12.6 s, 12.7 s, 14 s, and 14.5 s, respectively. From E to F, the motor has a velocity of 1.4 m/s, and from G to H, its velocity is 0.28 m/s. Since 0.14 m is the maximum value that the lower parts of the legs can be adjusted as from its mechanical design, the obstacle P is the maximal obstacle that the biped mechanism can overpass. Width and height of P are 0.07 m, and comparing them to Q, value 0.02 m of width and height, the capability of overcoming obstacle has been increased of 350% by using adjustable leg length.

Figure 21 shows contact forces of feet and chariot wheels with the ground as computed during the simulation in Fig. 18. Values are similar to those that are computed during the simulations of straight walking and changing directions.

Figures 22(a)–22(d) show the forces that are computed on the four translational joints of the shank sliders. It is worth to note that in the simulation, translational joints are activated for four slider pairs: one for the front part of the left shank, one for the rear part of the left shank, one for the front part of the right shank, and one for the front part of the right shank. However, in a real mechanism as illustrated in Fig. 2, there are two slider pairs for each of the above-mentioned parts. Thus, the real joint forces will be half of the forces in Fig. 22. Maximum values of the reaction forces at these four joints are computed to be less than 500 N when the chariot overpasses the obstacle. Thus, in a real prototype, the force of each translational joint will be less than 250 N. Since the sliders are chosen from market solutions made of aluminum alloy with high stiffness and strength, these values can be considered in proper ranges for a feasible operation. Simulation results of the forces at the LCCJ,

https://doi.org/10.1017/S0263574714000897 Published online by Cambridge University Press

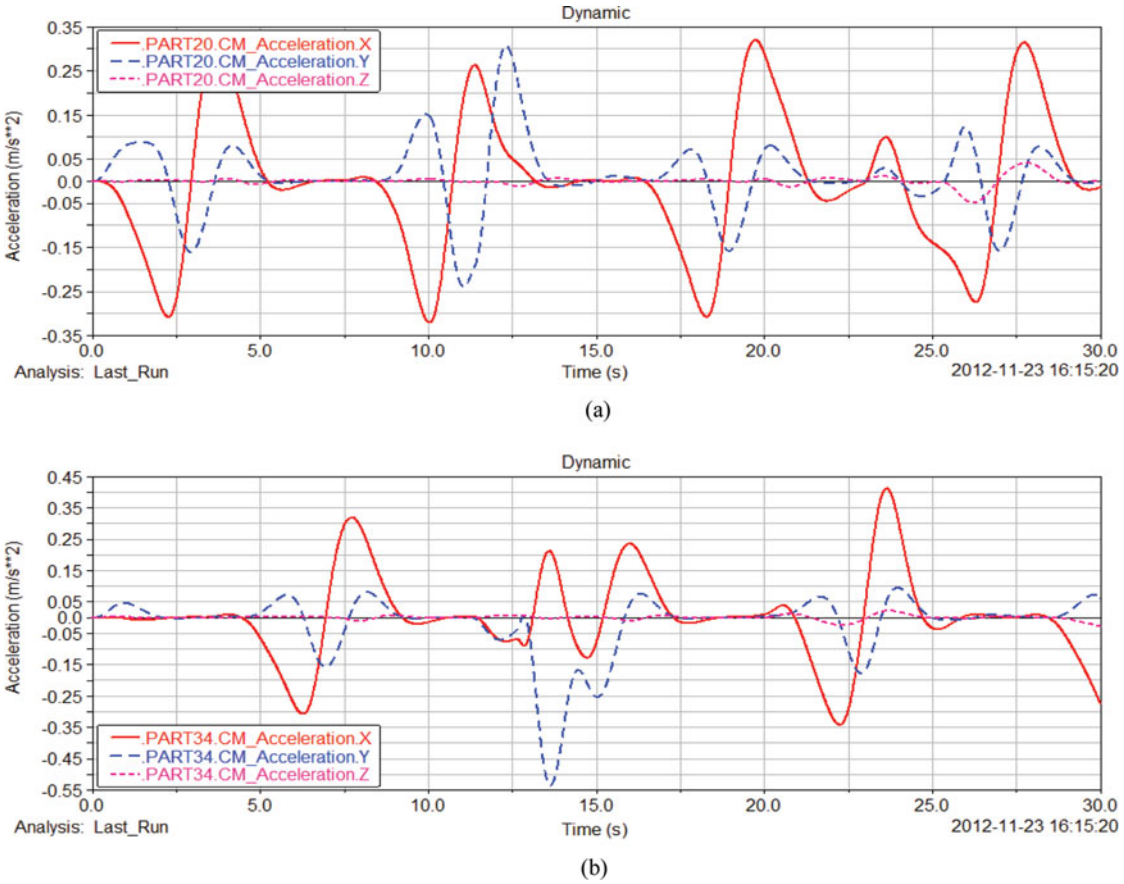

Fig. 24. *x*, *y*, and *z* components of CM acceleration as computed during the simulation in Fig. 18: (a) the left foot CM acceleration; (b) the right foot CM acceleration.

LCOJ, LKJ, and CCJ are omitted since there are no significant differences with the results that are obtained during the first two walking modes.

Figures 23(a) and 23(b) show the velocities of the left and right feet as computed in the simulation shown in Fig. 18, respectively. In addition, Figs. 24(a) and 24(b) show the corresponding accelerations. Maximum values of velocity and acceleration of the two feet are below 0.4 m/s and 0.55 m/s^2, respectively. Those values and the smooth curve indicate a good performance in overcoming obstacle.

Maximum values of the motor torques and critical constraints that are computed in simulations of the three walking modes are listed in Table II. These results can be considered reasonable for a practical operation and the leg motor torque is in accordance with Lagrange calculations that are reported in ref. [14]. The simulation results with the computed values and smooth behaviors give the possibility to choose market solutions for the motors and parts of the biped mechanism and its chariot since they can operate efficiently for the investigated operation modes.

4. Conclusions

A new LARM biped mechanism is presented with its CAD (computer-aided design) model and simulation results of basic operation modes. The solution has been conceived with low-cost easy-operation design by completing the walking system with a two-wheel chariot. The leg mechanism has been designed with a mobile shank carrying a wheel with the aim to give the possibility to have also wheeled locomotion mode and to increase the overpassing capability. Simulations are discussed with numerical results that show feasibility of the proposed design in the investigated operation

https://doi.org/10.1017/S0263574714000897 Published online by Cambridge University Press

Table II. Computed maximum values for motors and key joints[a].

Motors and constraints	Mode 1	Mode 2	Mode 3
1: motor torque for pulling/pushing left shank	–	–	1.6 Nm
2: motor torque for pulling/pushing right shank	–	–	1.7 Nm
3: motor torque for changing direction	–	7 Nm	–
4: right leg driving motor	8.8 Nm	9 Nm	10.4 Nm
5: left leg driving motor	8.8 Nm	11 Nm	10 Nm
A: left wheel-ground contact	140 N	135 N	143 N
B: right wheel-ground contact	140 N	130 N	141 N
C: left shank rear slider	–	–	400 N
D: left shank front slider	–	–	475 N
E: left foot-ground contact	190 N	185 N	188 N
F: right foot-ground contact	190 N	192 N	191 N
G: motor-gear connecting joint	–	700 N	–
H: leg-gear connecting joint	–	300 N	–
I: left Chebyshev crank joint	210 N	470 N	260 N
J: left Chebyshev output joint	350 N	345 N	360 N
K: left knee joint	200 N	350 N	388 N
L: chariot connecting joint	39 N	35 N	37 N

[a]In the table, numbers 1 to 5 and letters A to L are of Fig. 3.

modes. Those results are also used to characterize the operation of the proposed biped mechanism by stressing the advantages in having a mobile shank with a wheeled foot.

Acknowledgements

The first author wishes to acknowledge Chinese Scholarship Council for supporting his Ph.D. study and research at LARM in the University of Cassino and South Latium in Cassino (Italy) for the years 2010 to 2012.

References

1. M. Hirose, Y. Haikawa, T. Takenaka and K. Hirai, "Development of Humanoid Robot ASIMO," *Proceedings of the IEEE/RSJ International Conference on Intelligent Robots and Systems (IROS)-Workshop 2*, Maui, Hawaii (Oct. 29–Nov. 3, 2001) pp. 1321–1326.
2. K. Kaneko, F. Kanehiro, S. Kajita, H. Hirukawa, T. Kawasaki, M. Hirata, K. Akachi and T. Isozumi, "Humanoid Robot HRP-2," *Proceedings of the 2004 IEEE International Conference on Robotics & Automation*, New Orleans, USA (Apr. 26–May 1, 2004) pp. 1083–1090.
3. B. Verrelst, O. Stasse, K. Yokoi and B. Vanderborght, "Dynamically Stepping Over Obstacles by the Humanoid Robot HRP-2," *Proceedings of the 6th IEEE-RAS International Conference on Humanoid Robots*, Genova, Italy (Dec. 4–6, 2006) pp. 117–123.
4. K. Nishiwaki, S. Kagami, J. Kuffner, M. Inaba and H. Inoue, "Humanoid 'JSK-H7': Research Platform for Autonomous Behavior and Whole Body Motion," *Proceedings of the International Workshop Humanoid Human Friendly Robot (IARP)*, Tsukuba, Japan (Dec. 11–12, 2002) pp. 2–9.
5. J.-H. Oh, D. Hanson, W.-S. Kim, I.-Y. Han, J.-Y. Kim and I.-W. Park, "Design of Android type Humanoid Robot Albert HUBO," *Proceedings of the 2006 IEEE/RSJ International Conference on Intelligent Robots and Systems,* Beijing, China (Oct. 9–15, 2006) pp. 1428–1433.
6. I.-W. Park, J.-Y. Kim, J. Lee and J.-H. Oh, "Mechanical design of the humanoid robot platform HUBO," *Adv. Robot.* **21**(11), 1305–1322 (2007).
7. Z. Lige and H. Qiang, "A Visual Tele-Operation System for the Humanoid Robot BHR-2," *Proceedings of the 2006 IEEE/RSJ International Conference on Intelligent Robots and Systems*, *IROS'2006*, Beijing, China (Oct. 9–15, 2006) pp. 1110–1114.
8. Y. Ogura, H. Aikawa, K. Shimomura, H. Kondo, A. Morishima, H. Lim and A. Takanishi, "Development of a New Humanoid Robot WABIAN-2," *Proceedings of the 2006 IEEE International Conference on Robotics and Automation*, Orlando, USA (May 15–19, 2006) pp. 76–81.
9. E. Corral, J. Meneses and J. C. G. Prada, "Inverse and Forward Dynamics of the Biped Pasibot," *Proceedings of the 4th International Symposium on Multibody, Systems and Mechatronics (MUSME 2011)*, Valencia, Spain (Oct. 25–28, 2011) pp. 11–27.
10. Biped Robot Research at MEL (2012), available at http://staff.aist.go.jp/s.kajita/biped-e.html.

11. T. Li and M. Ceccarelli, "Additional Actuations for Obstacle Overcoming by a Leg Mechanism," *Proceedings of the 18th World Congress of the International Federation of Automatic Control (IFAC 2011)*, Milano, Italy (Aug. 28–Sep. 2, 2011) pp. 6898–6903.
12. T. Li and M. Ceccarelli, "An Experimental Characterization of a Rickshaw Prototype," *Int. J. Mech. Control* **12**(2), 29–38 (2011).
13. C. H. Liang, M. Ceccarelli and Y. Takeda, "Operation Analysis of a One-DOF Pantograph Leg Mechanism," *Proceedings of the 17th International Workshop on Robotics in Alpe-Adria-Danube Region RAAD08*, Paper no. 50, Ancona, Italy (May 25–27, 2008) pp. 15–17.
14. T. Li, "Design and Characterization of a New Biped Research Platform" *Ph.D. Thesis* (Cassino, Italy: University of Cassino and South Latium, 2013).

https://doi.org/10.1017/S0263574714000897 Published online by Cambridge University Press